*Oxidation of Metals, Vol. 44, Nos. 1/2, 1995*

# Oxidation of Multicomponent Two-Phase Alloys

**F. Gesmundo* and B. Gleeson†**

*Received October 15, 1994; revised December 8, 1994*

*The high-temperature corrosion behavior of two-phase alloys presents a number of differences compared to that of single-phase alloys. These differences are mainly a consequence of the limitations that the presence of two phases impose on the diffusion of the alloy components. In this review, it is shown that the exclusive scale formation of the more stable, slow-growing oxide is more difficult on a two-phase alloy, requiring a higher concentration of the more reactive alloy component than for a corresponding single-phase alloy. The main types of corrosion behavior for binary two-phase alloys are also considered, showing that if diffusion in the alloy is slow the scale structure will closely reflect that of the starting material. When diffusion in the alloy is not negligible, the scale structure becomes similar to what forms on single-phase alloys. The oxidation of two-phase ternary alloys is shown to be even more complex than the two-phase binary alloys. The principal added complexity compared to the binary alloys is that diffusion in the ternary alloys may also occur in the presence of two metal phases, as a result of an extra degree of freedom in the ternary system. The oxidation behavior of two-phase ternary alloys is discussed in the context of a number of recent experimental results.*

**KEY WORDS:** multiphase alloy oxidation; depletion zone; reservoir effect; diffusion path.

## INTRODUCTION

The high-temperature corrosion of metallic materials has been the topic of extensive research for over the last half-century. Much of this research has

*Istituto di Chimica, Facoltà di Ingegneria, Università di Genova, Fiera del Mare, Pad. D, 16129, Genova, Italy.
†School of Materials Science and Engineering, The University of New South Wales, Sydney, 2052, Australia.



0030-770X/95/0800-0211$07.50/0 

been concerned with the corrosion of pure metals and single-phase alloys in single-oxidant environments, such as oxygen or sulfur.[1-4] It is well established that there are numerous reaction modes which may exist within such relatively simple metal–environment systems; however, the fundamental principles underlying both the kinetics and thermodynamics of these reaction modes are fairly well understood. By contrast, when either the nature of the metallic material or that of the corroding environment becomes more complex, our ability to predict the actual corrosion behavior becomes quite limited. This is primarily because there are many more variables associated with corrosion in the more complex metal–environment systems. Further, fundamental research on the corrosion processes in more complex metal–environment systems has been quite limited.

Only a relatively small number of fundamental studies have been conducted on the high-temperature corrosion behavior of multiphase alloys.[5-15] This is quite surprising in view of the fact that multiphase alloys represent a class of materials used for many high-temperature, commercial applications. For example, high-temperature materials such as nickel- and cobalt-base superalloys, metal-matrix composites and many high-temperature metallic coatings, contain two or more phases.[1,16-18] In more recent years there has been a considerable amount of interest in intermetallic alloys due to their exceptionally high strength-to-weight ratios at high temperatures and consequent potential for numerous high-temperature applications.[19] Intermetallic alloys are often two-phase, or may even develop a second phase during reaction with the environment at high temperature.[20]

The aim of this paper is to review the current level of understanding of the high-temperature corrosion behavior of multiphase alloys. In view of the complexity of this topic, it is not possible to provide comprehensive review in the limited amount of space provided. Thus, attention will be restricted to only binary and ternary two-phase alloys corroded by a single oxidant. The oxidant will be assumed to be oxygen, although the following analysis could also apply to any other single oxidant.

## BACKGROUND

Previous studies on the high-temperature corrosion of multiphase alloys have been primarily concerned with general corrosion behavior in relation to corrosion kinetics and resulting scale morphologies.[21-36] Only rarely did these studies attempt to either analyze or even predict the differences in corrosion behavior between multiphase alloys and comparable single-phase alloys.[33-36] It is generally agreed, however, that a common mechanism to account for the high-temperature corrosion behavior of multiphase alloys does not exist. Examples of the various corrosion behaviors observed for

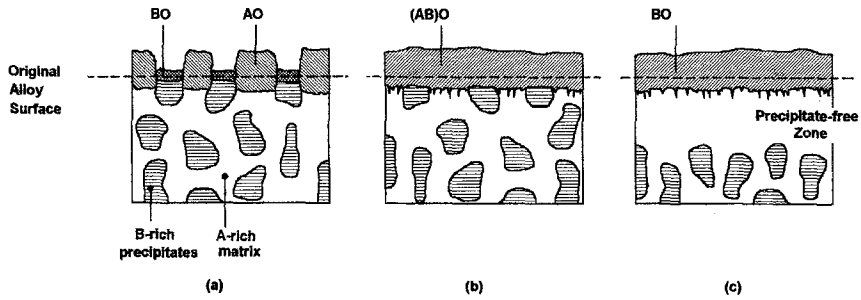


**Fig. 1.** Examples of the various corrosion behaviors observed in two-phase alloys for which each phase forms an outward-growing scale. (a) The two phases oxidize independently to form a nonuniform scale. (b) The two phases oxidize cooperatively to form a uniform scale. (c) The solute-rich second phase acts as a reservoir for the continued growth of the solute scale.

the case of two-phase alloys, and for which each phase forms an outward-growing scale, are shown schematically in Fig. 1. It is seen that in some cases, each phase in the two-phase alloy oxidizes independently to form a nonuniform scale (Fig. 1a[21,22,26,29]); whereas in other cases, the two alloy phases oxidize cooperatively to form a uniform scale (Fig. 1b[32,33]). Still, in another case, the solute-rich second phase acts as an effective solute reservoir for the continued exclusive growth of the solute–metal oxide scale (Fig. 1c[25,27,31,36]). An extension of this *reservoir effect* is the accumulation of solute-rich second-phase particles at the alloy–scale interface as a consequence of metal consumption.[37–39] In this case, the amount of particles which accumulate eventually becomes sufficiently high to result in the formation of a continuous scale layer of the solute–metal oxide. Such an *accumulation effect* would appear to be limited to only those systems in which either the matrix phase forms a volatile oxide (e.g., molybdenum) or the solubility of the solute element in the base-metal oxide is extremely low (e.g., silicon in NiO).

The alloy systems that will be examined in this paper are composed of two phases in which each phase contains all of the alloy components, but at different concentrations. Under equilibrium conditions, the activity of a given component is the same in the two phases, regardless of the extent to which the component concentrations differ. Thus, from the standpoint of equilibrium thermodynamics, the two alloy phases should exhibit equilibrium with the same oxide scale. An example of this is given in the 1100°C equilibrium isotherm of the Ti–Al–O system[40] in Fig. 2, where it is seen that two-phase alloys such as $Ti_3Al + TiAl$ and $TiAl + TiAl_2$ exhibit three-phase equilibrium with $Al_2O_3$.

In practice, however, the ideal situation of complete equilibrium is rarely observed. For example, preferential consumption of an alloy component

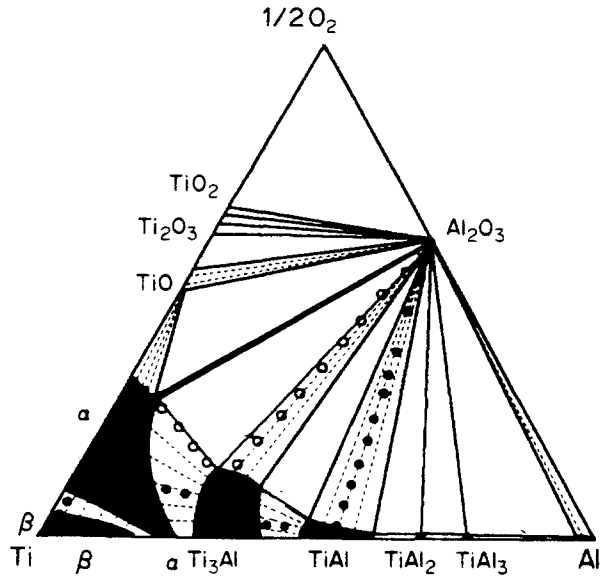


**Fig. 2.** The 1100°C equilibrium isotherm of the Ti–Al–O system.[40]

during oxidation may produce local changes in the average alloy composition in the corrosion-affected region which, in turn, may result in the disappearance of a phase or the appearance of a new phase. Such changes in the alloy phase constitution may result in changes in the type of corrosion product which forms and consequently affect the overall corrosion kinetics. Deviation from equilibrium may also occur when the oxidation behavior of the individual phases is significantly different. Such a difference is dictated primarily by the availability of the alloy component in a given phase to kinetically establish and then maintain the growth of its oxide scale. In the case of the oxidation of a $Ti_3Al + TiAl$ alloy, the $Ti_3Al$ has a lower aluminum content than TiAl, and one would therefore expect that it would be more difficult for the $Ti_3Al$ to establish and subsequently maintain $Al_2O_3$ scale growth. Indeed, it has been found[41] that the oxidation of $Ti_3Al$ at 850°C in dry oxygen results in the formation of primarily $TiO_2$, whereas the oxidation of TiAl under the same conditions results primarily in $Al_2O_3$ formation, and a two-phase, $Ti_3Al + TiAl$ alloy results in nonprotective, $TiO_2 + Al_2O_3$ scale formation.

Theoretical treatments of the oxidation of two-phase alloys have been presented by Wahl,[5] Wang *et al.*,[7] Wang,[8] and Gesmundo *et al.*[10–12] All of these treatments are semiquantitative in nature and are concerned primarily

with the case of the second phase, B-rich precipitate acting as a reservoir for BO scale formation (as in Fig. 1c). The treatments differ primarily in the assumption of steady-state[5] or non-steady-state[7,11] diffusion in the alloy, and whether or not the second-phase precipitates dissolve in an independent, nonuniform manner[7] or in a cooperative, uniform manner.[5,10–12] In the case of independent precipitate dissolution, it is assumed that a driving force exists for precipitates deeper within the alloy to dissolve, thus resulting in the development of a nonplanar, precipitate-dissolution front.

It is important to note that precipitate dissolution will occur only when the composition of B in the matrix phase decreases below the level required for precipitate–matrix equilibrium to be maintained (i.e., below the solubility limit). At relatively high precipitate volume fractions, the precipitates deeper within the alloy (but still close to the alloy–scale interface) would tend to be stable and would therefore not contribute to the scale formation. Thus, any treatment which considers precipitate dissolution to occur in an independent, nonuniform manner (see Wang *et al.*[7]) implicitly assumes that the precipitate volume fraction is quite small.

If the precipitate volume fraction is relatively high, then precipitate dissolution is expected to occur in a cooperative, uniform manner to result in the formation of a planar, precipitate-dissolution front. Indeed, such a precipitate-dissolution front would be favored by the lateral diffusion of the alloy components in the region of transition between the single- and two-phase zones. This is because lateral diffusion would tend to average out the alloy composition in directions parallel to the alloy surface. The development of a planar, precipitate-dissolution front was reported by Petkovic-Luton and Ramanarayanan,[42] who found that the composition of a 25Cr–20Ni alloy containing chromium-rich carbides (i.e., $M_{23}C_6$) changed abruptly from the bulk composition to a chromium-depleted composition upon crossing the interface separating the two-phase, bulk alloy structure and the single-phase, carbide-denuded zone.

## A SIMPLIFIED TREATMENT OF TWO-PHASE ALLOY OXIDATION

A simplified treatment of two-phase alloy oxidation will now be presented for the purpose of highlighting the important alloy parameters associated with the criterion for the exclusive formation of a protective scale. The treatment which will be presented is a modification of that presented by Wahl.[5]

Consider a two-phase alloy of bulk composition $X_o$, where $X_o$ is the mole fraction of component B in the alloy. It is assumed that the alloy contains B-rich precipitates of composition $X_p$ in a matrix of composition

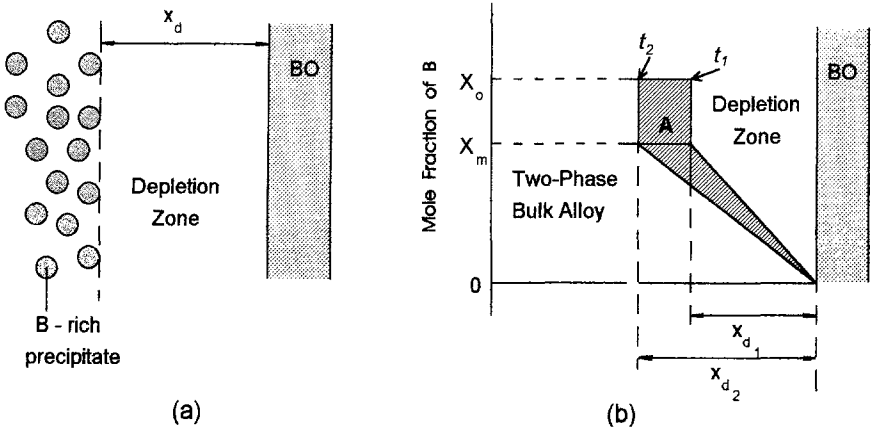


**Fig. 3.** (a) A schematic of the two-phase structure being analyzed; and (b) the assumed change in the composition profile after the time interval $t_1$–$t_2$.

$X_m$, where, similar to $X_o$, the compositions are in mole fraction of component B. As shown in Fig. 3a, it is further assumed that the alloy has oxidized to form an exclusive BO scale together with a near-surface precipitate-free zone of thickness $x_d$. Figure 3b shows the assumed steady-state change in the composition of the near-surface region of the alloy after an oxidation time interval of $(t_2-t_1)$, in which the concentration profile of B is assumed linear for simplicity. It is seen that in this time interval the depletion zone has increased in thickness from $x_{d_1}$ to $x_{d_2}$. The shaded area in this figure represents the amount of B that has gone to form BO in this time increment of $(t_2-t_1)$. Taking the alloy–scale interface to be immobile and the alloy concentration of B at this interface to be essentially zero (due to the high stability of BO), it can be easily shown that the shaded area, $A$, is given as

$$A=\frac{2X_o-X_m}{2}(x_{d_2}-x_{d_1}) \tag{1}$$

Thus, in the limit $(t_2-t_1)=dt$ and $(x_{d_2}-x_{d_1})=dx_d$, the steady-state flux of B to the alloy surface is given as

$$j_B=\frac{1}{2V_{all}}(2X_o-X_m)\frac{dx_d}{dt} \tag{2}$$

where $V_{all}$ is the molar volume of the alloy. It is noted that in Wahl's treatment, the flux of B to the alloy surface was approximated to be

$$j_B=\frac{1}{V_{all}}X_o\frac{dx_d}{dt}$$

The limitation of this approximation is that it does not account for the fact that the matrix contains B at a composition $X_m$.

From Fick's first law, the steady-state flux of B to the alloy surface in the linear profile approximation is also given as

$$j_B = \frac{1}{V_{all}} D_B \frac{X_m}{x_d} \tag{3}$$

where $D_B$ is the diffusivity of B in the precipitate-free zone of thickness $x_d$. Equating (2) and (3) and integrating, one obtains

$$x_d = \left( \frac{4 D_B X_m t}{2X_o - X_m} \right)^{1/2} \tag{4}$$

and substituting (4) into (3) gives

$$j_B = \left[ \frac{D_B X_m (2X_o - X_m)}{4 V_{all}^2 t} \right]^{1/2} \tag{5}$$

Under steady-state conditions the flux of B to the metal surface must be equal to the flux of B in the BO scale. Thus,

$$j_B = \frac{1}{V_{ox}} \left( \frac{k_p}{t} \right)^{1/2} \tag{6}$$

where $V_{ox}$ is the molar volume of the oxide BO (in $cm^3$/mole B) and $k_p$ is the parabolic rate constant for the BO scale growth in terms of scale thickness ($cm^2$/s). Equating (5) and (6) one obtains a criterion for the exclusive formation of BO in a two-phase alloy containing B-rich precipitates, i.e.,

$$[X_m(2X_o - X_m)]^{1/2} \geq [X_m(2X_o^*(\mathrm{II}) - X_m)]^{1/2} = \frac{2V_{all}}{V_{ox}} \left( \frac{k_p}{D_B} \right)^{1/2} \tag{7}$$

where $X_o^*(\mathrm{II})$ is the critical mole fraction of B in the bulk, two-phase alloy. In the case of a single-phase alloy $X_o = X_m$, so that Eq. (7) reduces to Wagner's criterion for the critical concentration of B ($X_o^*(\mathrm{I})$) necessary for the exclusive formation of BO on a single-phase binary alloy AB;[43]

$$X_o \geq X_o^*(\mathrm{I}) = \frac{2V_{all}}{V_{ox}} \left( \frac{k_p}{D_B} \right)^{1/2} \tag{8}$$

Equation (7) can be further modified so that it includes the precipitate volume fraction ($f_v$) as a parameter. This is done by noting that from the lever rule (and disregarding any differences in molar volumes)

$$f_v = \frac{X_o - X_m}{X_p - X_m} \tag{9}$$

and

$$X_o = X_m + f_v(X_p - X_m) \tag{10}$$

Substitution of these relationships into Eq. (7) gives

$$[X_m\{X_m + 2f_v(X_p - X_m)\}]^{1/2} \geq \frac{2V_{all}}{V_{ox}}\left(\frac{k_p}{D_B}\right)^{1/2} \tag{11}$$

Equation (11) highlights both the complexity and the important variables associated with multiphase alloy oxidation. It shows that, as a first approximation, the important variables for protective BO scale formation on a two-phase alloy containing B-rich precipitates are the precipitate and matrix compositions, the precipitate volume fraction, the growth rate of the solute oxide, and the solute diffusivity in the precipitate-free zone. The validity of Eq. (11) is substantiated qualitatively by the results of El Dahshan *et al.*,[36] who found that $Cr_2O_3$ formation on $Co + Cr_{23}C_6$ alloys oxidized in air at 900, 1000, and 1100°C, was determined by the chromium availability (i.e., $X_m$, $X_p$, and $f_v$) and not the chromium activity (as suggested by equilibrium thermodynamics).

Other variables which are not contained in Eq. (11), but which intuitively may be thought to play a role, are precipitate size and distribution, precipitate dissolution kinetics, and the oxidation kinetics of the matrix phase. Protective scale formation is expected to be more difficult if the precipitate distribution is nonuniform, the precipitate dissolution kinetics are slow, or the oxidation kinetics of the matrix phase are high. With regard to precipitate size, Wang *et al.*[7] concluded that the ratio of precipitate volume fraction to precipitate size (i.e., $f_v/r$) must exceed a critical value in order to ensure exclusive formation of the solute–metal oxide on the two-phase alloy. The implication of this conclusion is that a decrease in the precipitate size helps to promote formation of the protective solute scale. Clearly, this effect is a characteristic of two-phase alloys and does not exist for single-phase alloys, for which only a change of the alloy grain size can have an effect of improving its ability to form a protective scale.[4] Recent experimental results on the oxidation of two-phase alloys containing intermetallic compounds in the Ti–Al system[44] are in agreement with Wang *et al.*'s conclusion. It was found that the oxidation behavior of an alloy with a fixed average

composition is critically dependent on the size of the Al-rich precipitate phase. Specifically, when the Al-rich precipitates were small, alloys with a sufficient aluminum content could form a protective $Al_2O_3$ scale, while the same alloys containing larger precipitates tended to form a nonprotective, $Al_2O_3 + TiO_2$ scale.

A quantitative comparison between Eq. (8) and either Eq. (7) or (11) reveals that protective scale formation is generally more difficult on a two-phase alloy than on a single-phase alloy, particularly if the solubility limit of B in the matrix phase ($X_m$) is quite low. It is noted that in such a comparison it is assumed that the diffusivity of solute metal B is the same in both alloy structures. The difference in the scaling behavior of the two alloy structures can be most easily shown by equating Eqs. (7) and (8) such that

$$[X_m(2X_o^*(\mathrm{II}) - X_m)]^{1/2} = X_o^*(\mathrm{I}) \tag{12}$$

For a two-phase alloy, we can write $X_m = X_o^*(\mathrm{II})r$, where $r$ is a parameter which is less than unity (i.e., $0 < r < 1$). Thus, Eq. (12) can be rewritten as

$$(2r - r^2)^{1/2}[X_o^*(\mathrm{II})] = X_o^*(\mathrm{I}) \tag{13}$$

or

$$\frac{X_o^*(\mathrm{II})}{X_o^*(\mathrm{I})} = \frac{1}{(2r - r^2)^{1/2}} \propto \frac{1}{(X_m)^{1/2}} \qquad (\text{for } r \ll 1) \tag{14}$$

Equation (14) shows that as $X_m$ decreases, $X_o^*(\mathrm{II})$ becomes much larger than $X_o^*(\mathrm{I})$. In fact, it is even possible that $X_o^*(\mathrm{II})$ may fall within the stability range of the B-rich phase, so that exclusive formation of the protective scale will not occur on the two-phase alloy.

The conclusion that protective scale formation is generally more difficult on a two-phase alloy than on a single-phase alloy is in agreement with a recent theoretical analysis by Gesmundo *et al.*[12] on the oxidation behavior of two-phase binary alloys. The conclusion is further supported experimentally by the results of a study on the oxidation behavior of (in weight %) Fe–15Cr and Fe–15Cr–1C alloys.[45] As shown in Fig. 4, the single-phase Fe–15Cr alloy formed a protective, $Cr_2O_3$ scale layer when oxidized in air for 72 h at 850°C, whereas the Fe–15Cr–1C alloy, which has a two-phase, $\gamma$-Fe + $(Cr,Fe)_{23}C_6$ microstructure, does not form a protective $Cr_2O_3$ scale. Rather, the scale which formed on the two-phase Fe–15Cr–1C alloy consisted of an outer layer of the iron oxides (primarily FeO) and a thick, multiphase inner layer of $FeO + FeCr_2O_4$. Clearly, the inability of the Fe–15Cr–1C alloy to form a $Cr_2O_3$ scale is attributable to the chromium being tied up as carbides and the consequent reduction in the chromium availability, i.e., the *multiphase effect*.

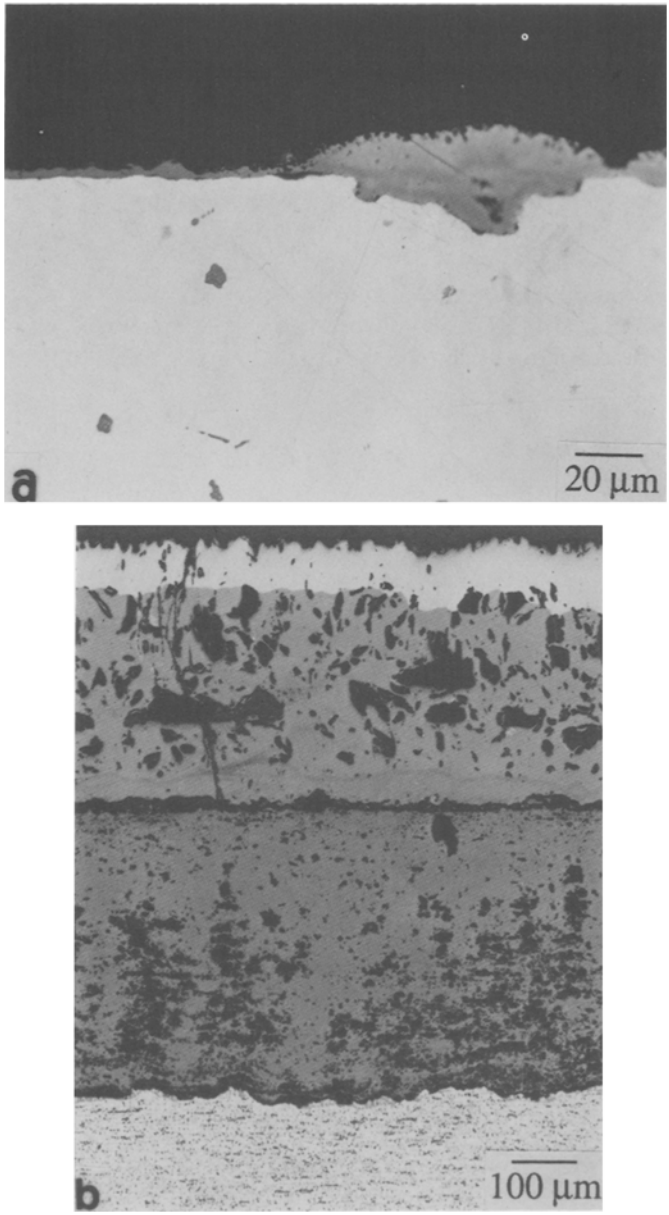


**Fig. 4.** Optical micrographs of (in weight %) (a) Fe–15Cr and (b) Fe–15Cr–1C alloys after 72 h oxidation in air at 850°C. The Fe–15Cr alloy is single phase while the Fe–15Cr–1C alloy is two phase, consisting of $(Cr,Fe)_{23}C_6$ precipitates in a $\gamma$-Fe matrix.

The present analysis is also in agreement with the analyses by Wahl[5] and Wang *et al.*[7] These authors concluded that the critical concentration of the protective-scale-forming element (e.g., chromium or aluminum) is lower in the matrix phase of a two-phase alloy compared to that of a single-phase alloy. It should be noted, however, that although this is theoretically true, the present analysis does indicate that there must also exist a limit on how low $X_m$ can be. From Eq. (11), the value of this limit should depend on the values of $f_v$ and $X_p$.

In the following, the oxidation behavior of two-phase binary and ternary alloys shall be discussed separately. Particular attention will be given to two-phase binary alloys. Moreover, the analysis of the two-phase binary alloys will be concerned mainly with theoretical predictions of the possible types of scale structures. This is done because systematic experimental investigations of the corrosion behavior of binary (and ternary) two-phase alloys have not yet been presented in the open literature. Only a few actual examples will be referred to in which some of the oxidation modes expected on the basis of a theoretical analysis have actually been observed.

## THE OXIDATION OF TWO-PHASE BINARY ALLOYS

The principal case which will be considered for the binary alloys is that of two metal components, A (the most noble) and B (the most reactive), which exhibit limited solubility in each other and do not react to form intermediate phases. The solid solutions of B in A and of A in B shall be denoted as $\alpha$ and $\beta$, respectively. A schematic isothermal phase diagram of a hypothetical ternary A–B–O system is shown in Fig. 5. In this system, it is assumed that the two oxides are completely insoluble in one another and that BO is much more stable than AO. As a consequence of the latter assumption, the alloy composition in simultaneous equilibrium with the two oxides is located in the $\alpha$-phase field. The oxygen pressures corresponding to the various invariant points in the diagram are denoted as $P_1$ ($\alpha$ + AO + BO equilibrium), $P_2$ (A + AO equilibrium), $P_3$ ($\alpha + \beta$ + BO equilibrium), and $P_4$ (B + BO equilibrium).

The two fundamental cases of two-phase, binary-alloy corrosion by a single oxidant to be examined correspond to an oxidant partial pressure which is either below the stability of the least-stable oxide (low oxidant pressures) or above it (high oxidant pressures). Under low oxidant pressures the two limiting situations of either the internal or external oxidation of B will be considered; while under high oxygen pressures the three possible situations of external oxidation of A coupled with the internal oxidation of B, the mixed external oxidation of A and B, or the exclusive external oxidation of B, will be considered.

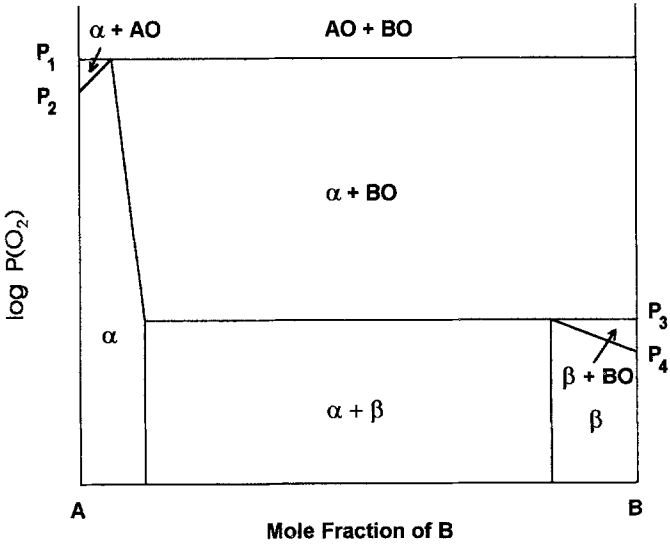


**Fig. 5.** An isothermal phase diagram of the hypothetical A–B–O system.

## Oxidation Modes of Two-Phase Binary Alloys Under Low Oxidant Pressures

The oxidation behavior of two-phase binary alloys under low oxidant pressures depends critically on the solubility and diffusivity of B in the $\alpha$ phase, and on the alloy microstructure. With regard to alloy microstructure, the following two limiting conditions may be distinguished:[13,14]

(i) An $\alpha$-phase matrix containing a distribution of $\beta$-phase precipitates—*$\alpha$-matrix alloys*; or
(ii) A $\beta$-phase matrix containing a distribution of $\alpha$-phase precipitates—*$\beta$-matrix alloys.*

An analysis of the conditions for the transition from internal to external oxidation of B in $\alpha$-matrix alloys, assuming that the reaction is controlled by the diffusion of O and B through the $\alpha$ phase, leads to the conclusion that the transition is more difficult in two-phase alloys compared to single-phase alloys.[15] In fact, the critical value of the average concentration of B required for this transition in two-phase alloys is larger than for single-phase alloys under the same values of all the relevant parameters. Moreover, the transition becomes more difficult as the solubility of B in the $\alpha$ phase decreases, until, for sufficiently low solubilities of B in A, only internal BO formation will occur. This latter case will be discussed first, followed by the case of external BO formation.

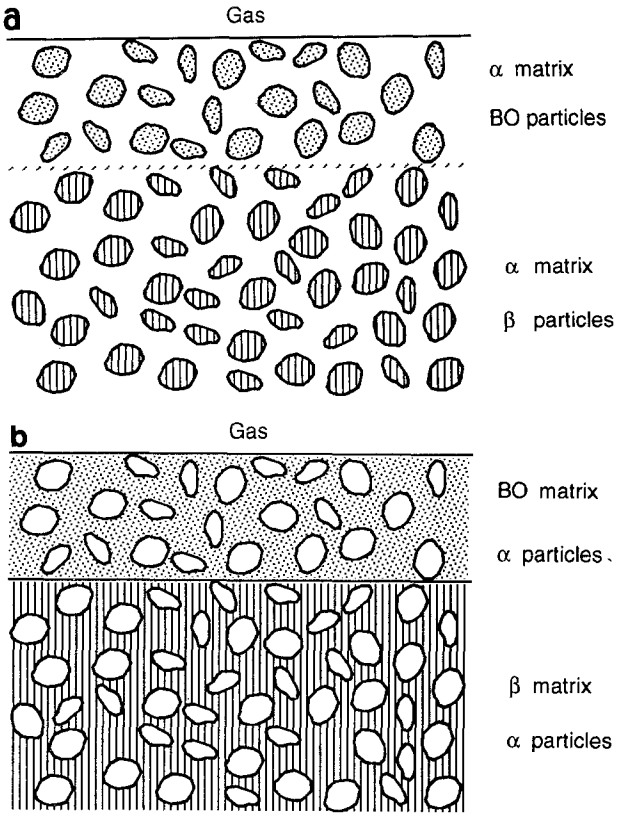


**Fig. 6.** Schematic structure of the scales formed on two-phase binary A–B alloys under low oxidant pressures and in the absence of diffusion processes of the metal components in the alloy: (a) $\alpha$-matrix alloy; and (b) $\beta$-matrix alloy.

If the solubility and diffusivity of B in the $\alpha$ phase are very small, the microstructure of the corroded region will closely follow that of the original alloy. In the case of $\alpha$-matrix alloys, an internal oxidation zone consisting of BO-rich islands in the $\alpha$ matrix will form. The distribution of the BO-rich islands would correspond to that of the $\beta$ precipitates in the bulk-alloy microstructure, as shown in Fig. 6a. This mode of internal oxidation may be referred to as *in situ* or *diffusionless*, since they occur without any appreciable diffusion of B. Diffusionless internal oxidation is commonly observed in two-phase alloys.[14]

In contrast to the $\alpha$-matrix alloys, the low $P_{O_2}$ oxidation of $\beta$-matrix alloys under conditions of very low solubility and diffusivity of B in the $\alpha$ phase is expected to produce a BO matrix containing a dispersion of $\alpha$-precipitates, as shown in Fig. 6b. The distribution of the $\alpha$-precipitates would

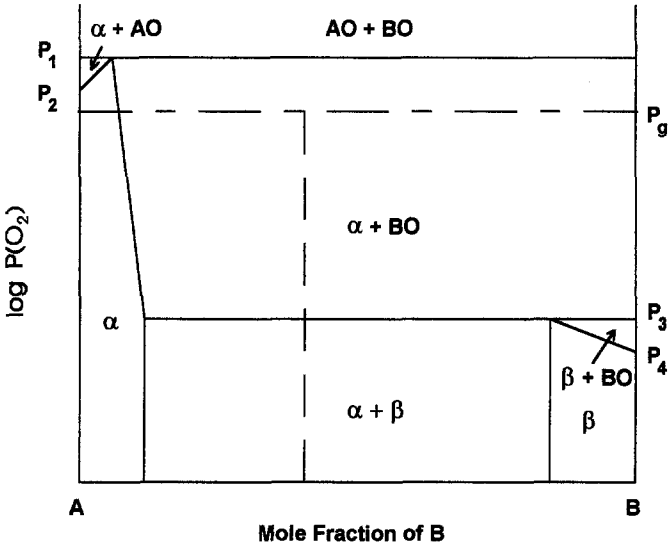


**Fig. 7.** The diffusion path corresponding to the expected scale structure resulting from a diffusionless internal oxidation process.

be the same as that in the bulk alloy. The structure of the scale would be similar to an exclusive BO scale formed on a single-phase alloy, with the only difference being the presence of $\alpha$-precipitates inside the BO scale of the two-phase alloy. Irrespective of this difference, however, the oxidation kinetics are expected to be controlled by the transport of matter through the BO scale.

The diffusion path corresponding to the expected scale structure resulting from a diffusionless internal oxidation process is shown in Fig. 7. It is seen that the diffusion path is simply a vertical line starting from the bulk-alloy composition, advancing through the two-phase, $\alpha + BO$ field, and ending at the oxygen pressure $P_g$ prevailing in the gas phase. Diffusionless internal oxidation will not produce any depletion of B in the alloy, so that the metal ratio, A:B, within the internal oxidation zone will be the same as in the original alloy. It may also be predicted that the size of both the BO and $\alpha$ precipitates generated as a consequence of the internal oxidation of the $\beta$ phase will be quite small. This is because the precipitate phases form by a solid-state reaction from a single phase, and should therefore involve only small displacements.[14]

Interesting examples of diffusionless internal oxidation under low oxidant pressures have been obtained recently in a study of the corrosion of Fe–Nb[46] and Co–Nb[47] alloys containing 15 and 30 wt.% Nb in $H_2$–$CO_2$ mixtures

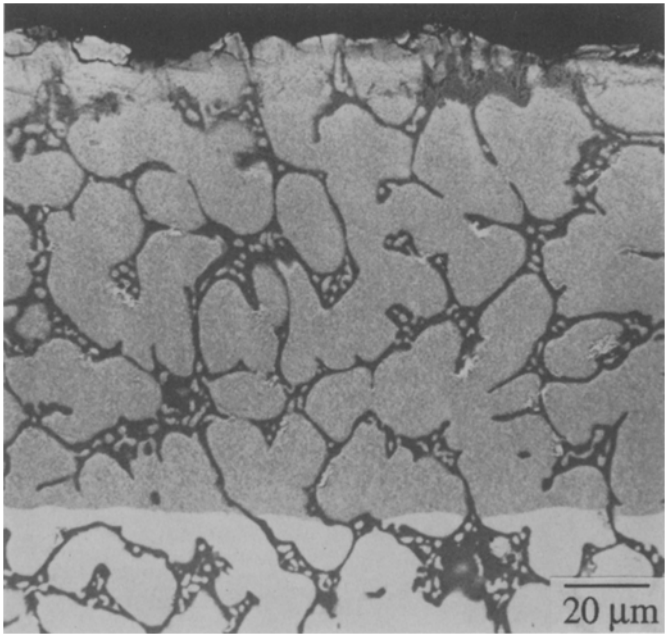


**Fig. 8.** Secondary electron image of a Fe–30 wt.% Nb alloy oxidized at 800°C in an $H_2$–$CO_2$ mixture which corresponded to an oxygen partial pressure below the stability of FeO.

at 600–800°C. Most of the alloys were two-phase, comprised of a solid-solution iron or cobalt matrix and large Nb-rich precipitates. The compositions of the Nb-rich precipitates were close to $Fe_2Nb$ for the iron-base alloys and to $Co_3Nb$ for the cobalt-base alloys, and the solubility of niobium in the solid-solution phases was very low. In the alloys oxidized at a $P_{O_2}$ below the stability of the base-metal oxides, the Nb-rich precipitates were converted into very fine mixture of niobium oxides ($NbO_2$ and $Nb_2O_5$) and base metal, while the solid-solution matrix phase was unaffected. An example of this is shown in Fig. 8 for the case of the Fe–30Nb alloy oxidized at 800°C under an oxygen partial pressure below the stability of FeO. The dark phase in the alloy is almost pure Fe, while the light phase is the intermetallic compound $Fe_2Nb$. The outer region the alloy has darkened due to the conversion of Nb into $NbO_2$ and $Nb_2O_5$. It is apparent that the distribution of niobium in this region is the same as that of the Nb-rich phase in the base alloy. Moreover, in accordance with a diffusionless internal oxidation process, no niobium depletion was observed beneath the region of internal oxidation.

A change in the structure of the oxidation zone relative to that of the bulk alloy should occur when the solubility and diffusivity of B in the $\alpha$

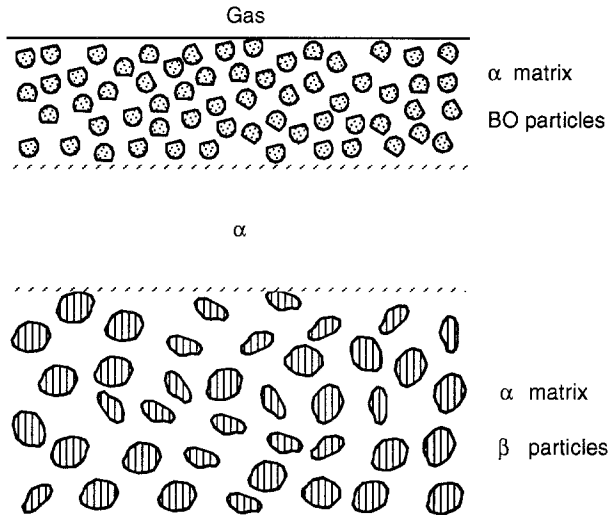


**Fig. 9.** Schematic structure of the corrosion-affected region after a low $P_{O_2}$ oxidation of a two-phase, $\alpha$-matrix alloy with a relatively low B content and in which the metal components in the alloy exhibit high diffusivities.

phase are relatively high. In fact, as a consequence of the preferential consumption of B, the alloy will become enriched in A, and possibly result in the formation of a $\beta$-depleted, $\alpha$ layer above the bulk, $\alpha+\beta$ structure. Two limiting situations may exist for the oxidation of two-phase alloys forming a $\beta$-depleted, $\alpha$ layer, depending on whether the oxidation of B occurs internally or externally. If the concentration of B in the alloy is small, internal BO formation will occur. This will lead to the development of an outermost layer composed of an $\alpha$-matrix containing isolated BO particles and an innermost $\alpha$ layer free of BO inclusions, as shown in Fig. 9 (for an $\alpha$-matrix alloy). It is the supply of B to the internal oxidation front which leads to the formation of this innermost $\alpha$ layer. Thus, the concentration profile of B across the innermost layer will decrease from the solubility limit of B in $\alpha$ ($X_m$) at the $\alpha/(\alpha+\beta)$ boundary to a value very close to zero at the $\alpha/(\alpha+$internal BO) boundary. The distribution of the internal oxide particles should be similar to what would be observed for the internal oxidation of single-phase alloys, i.e., a uniform BO particle distribution which has no correlation with the two-phase microstructure of the bulk alloy.

The resulting diffusion path corresponding to the structure obtained during this *diffusive* type of corrosion (Figs. 10 and 11) in which internal BO formation occurs is more complex than the diffusionless type considered in Fig. 7. In principle, the diffusion path should move horizontally from the

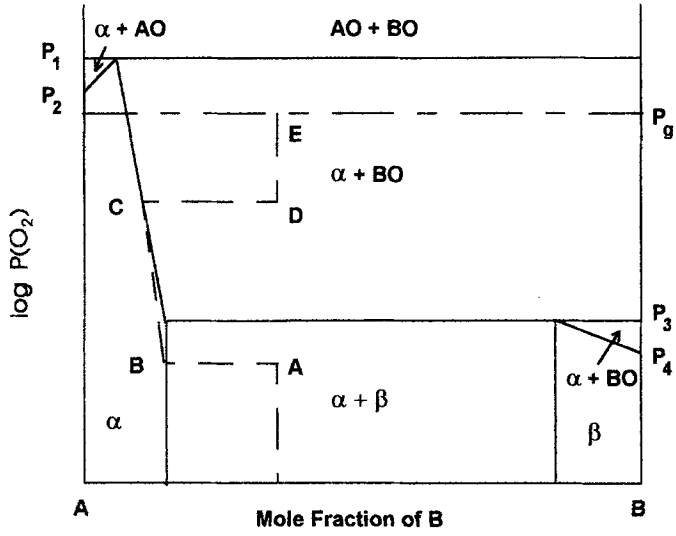


**Fig. 10.** The diffusion path corresponding to the expected structure resulting from a diffusive oxidation process in which only internal BO formation occurs.

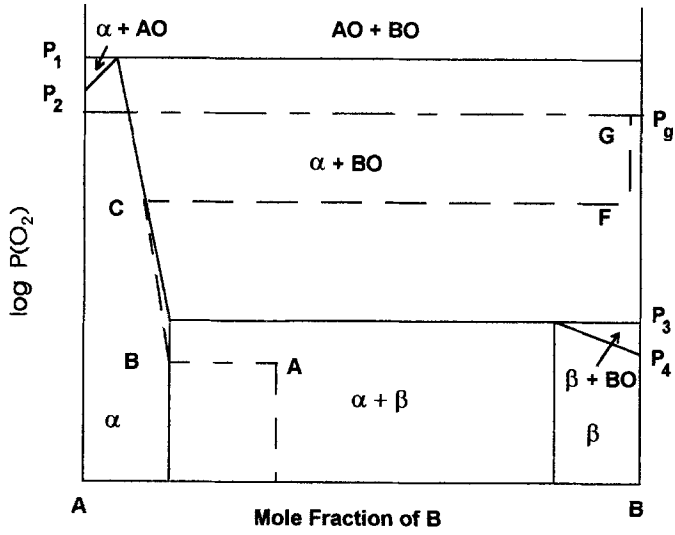


**Fig. 11.** The diffusion path corresponding to the expected structure resulting from a diffusive oxidation process in which both internal and external BO formation occurs.

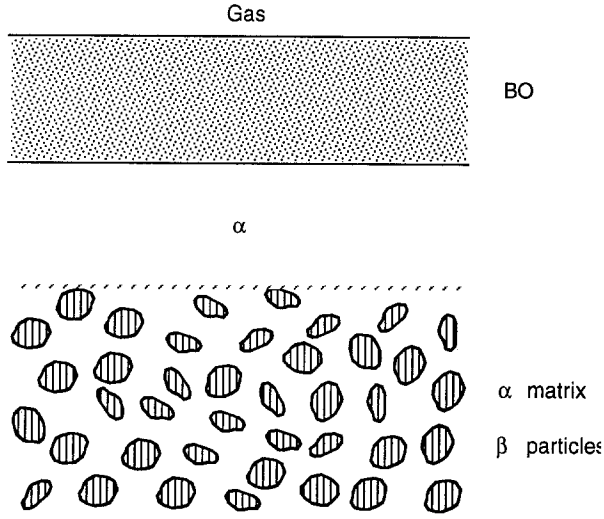


**Fig. 12.** Schematic structure of the corrosion-affected region after a low $P_{O_2}$ oxidation of a two-phase, $\alpha$-matrix alloy with a relatively high B content and in which the metal components in the alloy exhibit high diffusivities.

two phase, $\alpha+\beta$ field to the boundary of the single-phase $\alpha$ field at some oxygen pressure below $P_3$ (line A–B in Figs. 10 and 11), and then upwards with a negative slope until it contacts the $\alpha+$BO equilibrium boundary at some point C below $P_g$. The ensuing form of the diffusion path is dependent upon whether or not B is oxidized internally or externally. Figure 10 shows the case in which of only internal BO precipitation occurs. It is seen that the diffusion path moves horizontally in the two-phase $\alpha+$BO field up to a location close to the original alloy composition (point D) and then moves upwards vertically to $P_g$, following line D–E. In the case where external BO formation occurs as well, which is shown in Fig. 11, the diffusion path will move from point C to the extreme right of the diagram (point F), corresponding to the growth of pure BO, and then upwards vertically along F–G to $P_g$.

The second limiting situation will occur when the binary two-phase alloy is sufficiently rich in B to enable the formation of a BO scale, irrespective of the alloy microstructure, as shown in Fig. 12 for an $\alpha$-matrix alloy. For this, the solubility of B in the $\alpha$ phase must be higher than the critical concentration for the transition from internal to external scale formation. Similar oxidation behavior is expected for both $\alpha$- and $\beta$-matrix alloys which have overall B contents above the critical value.

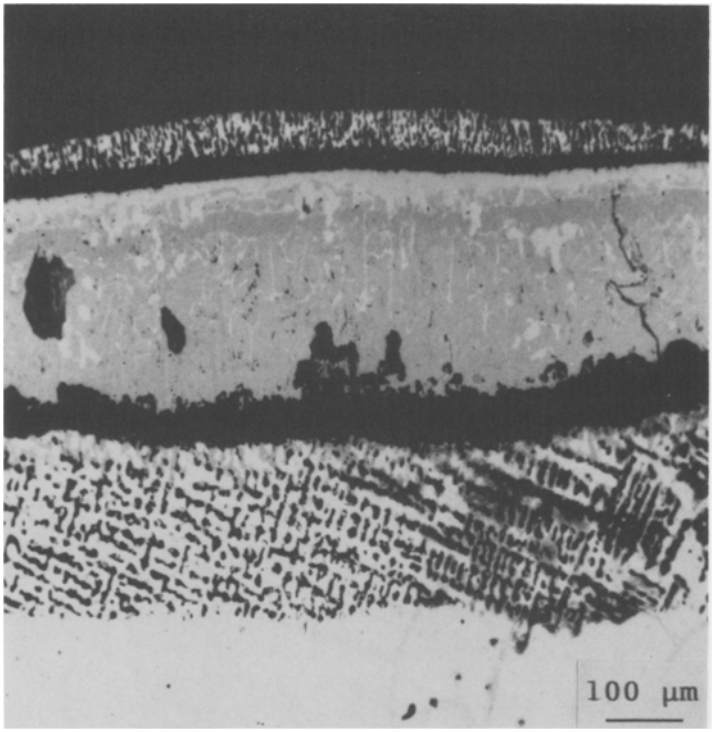


**Fig. 13.** Optical micrograph of a two-phase Fe–44 wt.% Cu alloy after oxidation at 1000°C and 1 atm oxygen. The internally oxidized region consists of oxidized iron particles (FeO) in a copper matrix.

## Oxidation Modes of Two-Phase Binary Alloys Under High Oxidant Pressures

The corrosion behavior expected for two-phase binary alloys under high oxidant pressures is more complex than under low oxidant pressures due to a larger variety of scale structures which may arise due to the added possibility of AO formation (the least stable oxide). If diffusion of B in the $\alpha$ phase is negligible, the corrosion of $\alpha$-matrix alloys under high oxidant pressures leads to the formation of external scales composed of an AO matrix containing a dispersion of BO particles. Underneath this outer scale, a layer of internally oxidized $\beta$ precipitates within the $\alpha$ matrix could also form.[13] The distribution of the BO particles in both the external scale and the region of internal oxidation will follow that of the $\beta$ precipitates in the alloy. Similar to the case considered in the previous section, this is a diffusionless internal oxidation process. As shown in Fig. 13, such an internal oxidation process

is observed in the oxidation of a two-phase Fe–44 wt.% Cu alloy under 1 atm oxidation at 1000°C.[48] Although not readily apparent in this figure, beneath the complex external scale, a region of internal oxidation exists in which the iron particles inside the Cu matrix have been converted into FeO.

The oxidation behavior represented in Fig. 13 is expected to occur if the oxidation rate of the $\alpha$ matrix is not very large in comparison to the rate of internal oxidation. The latter rate will depend not only on the diffusivity of oxygen in the $\alpha$ phase, as expected for the internal oxidation in single-phase alloys when the diffusion of B is very slow,[1,49] but also on the size and oxidation kinetics of the $\beta$ precipitates. The $\beta$ precipitates may oxidize at the alloy–scale interface simultaneously with the $\alpha$ matrix, in which case a region of internal oxidation will not form. Alternatively, the $\beta$ precipitates may survive for an extended period of time within the AO matrix. This latter scale structure is clearly not in thermodynamic equilibrium with respect to the oxidation of B and may appear only as a result of kinetic limitations for this reaction.

The presence of $\beta$ precipitates inside an AO matrix has been observed in the oxidation of Cu–Cr alloys[50,51] and in the sulfidation of M–Nb alloys (with M = Fe or Co) in sulfur vapor[52,53] and $H_2$–$H_2S$ mixtures.[54,55] The continued corrosion of $\beta$ precipitates inside an AO matrix will occur gradually with time. Moreover, the time required for their complete corrosion is inversely related to their size. This is because small precipitates have a larger surface area to volume ratio compared to large precipitates. In the case of the sulfidation of Fe–Nb alloys containing 15 and 30 wt.% Nb in $H_2$–$H_2S$ mixtures at 600–800°C,[54] the small $Fe_2Nb$ precipitates in the Fe–15Nb alloys were able to survive inside an inner FeS layer at only 600°C. By contrast, the much larger $Fe_2Nb$ precipitates in the Fe–30Nb alloy were able to survive inside the inner FeS layer for longer times and at higher temperatures (up to 800°C). The incorporation of $\beta$ precipitates into an inner AO layer will cause the supply of B to decrease from what would occur under the ideal conditions of complete precipitate dissolution. As a consequence, the effective total content of B in the alloy will be lowered because the amount of B which is contained in the oxide-incorporated, $\beta$ precipitates becomes inactive.

The corrosion of $\beta$-matrix alloys under high $P_{O_2}$ conditions should produce a BO scale containing AO particles in the outer region and $\alpha$ particles in the inner region. The $\alpha$ particles are present in the inner region of the BO scale where the oxygen activity varies between $P_1$ and $P_3$, so that AO formation is not thermodynamically possible. Only after the oxygen activity increases above $P_1$ at some point within the BO scale, will oxidation of the $\alpha$ particles take place. In both regions of the BO-matrix scale, the AO and $\alpha$ particles will show the same distribution as the $\alpha$-precipitates in the bulk alloy.

If the solubility and diffusivity of B in the $\alpha$ phase are relatively large, the oxidation of $\alpha$-matrix alloys under high oxidant pressures may result in one of three typical scale structures.[13] If the overall average concentration of B in the alloy is small, then similar to the low $P_{O_2}$ case, the corrosion of the two-phase alloys will produce a three-layered structure consisting of an external AO scale, followed by an intermediate layer of internal oxidation in which BO particles are embedded in substantially pure A, and then by an innermost $\beta$-depleted $\alpha$ layer. A mathematical treatment of the internal oxidation of B in the presence of an external AO scale on a two-phase alloy has not yet been developed. However, by analogy with the results obtained for the case of internal oxidation in the absence of an external AO scale,[15] it may be expected that the transition from internal oxidation of B to the formation of a mixed AO + BO scale will require a higher concentration of B in the two-phase alloy than in the single-phase alloy. It may also be expected that this transition will become more difficult when the solubility of B in the $\alpha$ phase is reduced.

If the overall concentration of B in the alloy is larger than the critical value required to prevent the internal oxidation of B, but too small to produce external BO exclusively, the resulting scale will consist of a mixture of the two oxides above a $\beta$-depleted $\alpha$ layer. Even in this case the scale structure will not follow that of the underlying alloy, since the original two-phase structure is lost due to the formation of the $\alpha$ layer. Finally, if the concentration of B in the alloy is sufficiently large, an exclusive external layer of pure BO may form on the two-phase alloy under a high oxidant pressure. Again, the outer BO scale layer will grow over a $\beta$-depleted $\alpha$ layer which will form as a result of the preferential consumption of B.

## THE OXIDATION OF TWO-PHASE TERNARY ALLOYS

As discussed in the previous section, the oxidation of two-phase binary alloys can lead to the formation of a single-phase metallic layer. When a two-phase ternary alloy is oxidized, however, the situation becomes more complex, and formation of a two-phase metallic layer becomes an added possibility. Moreover, the diffusion of the alloy components back into the ternary alloy must also be considered. The increased complexity associated with two-phase, ternary-alloy oxidation can be attributed to the extra degree of thermodynamic freedom as stipulated by the Gibbs phase rule.[56] Under isothermal and isobaric conditions, the Gibbs phase rule for a *binary alloy* AB is

$$f = 2 - p \tag{15}$$

where $f$ is the degree of freedom and $p$ is the number of phases. Thus, on the basis of Eq. (15) and disregarding the presence of oxygen (which is

reasonable unless the oxygen solubility in the alloy is very high), there can be no chemical-potential gradients to cause long-range diffusion in a two-phase binary alloy. As a consequence, it is not possible for component A to diffuse back into the two-phase alloy, even if it becomes enriched at the alloy–scale interface due to the selective oxidation of B. Therefore, apart from internal oxidation, the only possible phase transformation which may occur in a binary alloy is the destabilization of the two-phase structure to a single-phase structure (e.g., A-rich $\alpha$). By contrast, the Gibbs phase rule for a *ternary alloy* under isothermal and isobaric conditions is

$$f = 3 - p \tag{16}$$

In this case, one degree of freedom exists in a ternary alloy exhibiting two-phase equilibrium, and it is therefore possible for diffusion to occur through a two-phase structure. This can have the effect of significantly changing the alloy phase constitution and possibly increasing the corrosion kinetics. It is noted, however, that if the rates of component diffusion are very low, the ternary alloy will very likely oxidize in a diffusionless manner,[57] similar to what was discussed in the previous section for the case of binary alloys.

Ling *et al.*[9] have published the only computational treatment of two-phase, ternary-alloy oxidation in which component diffusion back into the alloy was considered. The system they modeled was a Ni–Cr alloy containing $Cr_{23}C_6$ precipitates. The alloy was assumed to form a carbide-free zone by the dissolution of carbide precipitates to supply chromium for the exclusive growth of a $Cr_2O_3$ scale. A computational simulation of this scale growth–precipitate dissolution combination showed that the carbon released by the $Cr_{23}C_6$ dissolution diffuses back into the alloy where it supersaturates the metal matrix to result in more carbide precipitation. Such behavior is in agreement with what has been observed experimentally during oxidation of various alloy + carbide systems.[36,42]

For ternary alloys in which each component is metallic, the oxidation-induced diffusion of the components can result in significant changes from the original alloy phase constitution.[30,34] However, prediction of the resulting phase changes is extremely difficult due to the large number of kinetic parameters involved. These kinetic parameters include the oxidation behavior of the alloy (i.e., the type of scale which forms) and the component diffusivities in the different alloy phases. Data for all these parameters for a given alloy system are typically not available. Thus, an understanding of the oxidation behavior of two-phase, all-metallic ternary alloys is still very dependent on experimental investigations. To date, however, only a limited number of such investigations have been reported.[30,34,58,59]

The complexity of two-phase, ternary alloy oxidation is best illustrated by considering the cyclic-oxidation behavior of a Ni–Cr–Al alloy comprised

of a nickel-rich $\beta$-NiAl matrix and $\alpha$-Cr precipitates.[30] The alloy was cyclically oxidized at 1100°C in still air, with each thermal cycle consisting of 1 h at temperature followed by 30 min in ambient. A cross section of the alloy after 136 cycles is shown in Fig. 14a. It is seen that extensive internal $Al_2O_3$ formation occurred and that the oxidation process resulted in phase transformations from the original $\alpha + \beta$ structure. The phase changes which occurred are represented in Fig. 14b, where the variation in the overall alloy composition is plotted as a diffusion path on the Ni–Al–Cr phase diagram. The diffusion path moves from the bulk $\alpha$-Cr + $\beta$-NiAl equilibrium to $\gamma$-Ni + $\beta$-NiAl equilibrium, and then to $\gamma$-Ni (+$Al_2O_3$) equilibrium. The phase transformations were initiated by the formation of a near-surface $\gamma$-Ni layer which resulted from the selective oxidation of aluminum to form an $Al_2O_3$ scale. A significant amount of aluminum depletion was possible because of the continual spallation and reformation of the $Al_2O_3$ scale. The internal $Al_2O_3$ formation occurred when the aluminum content in the $\gamma$-Ni layer decreased below about 10 at.%.

The development of the diffusion path shown in Fig. 14b did not occur solely as a consequence of aluminum depletion from the alloy. Rather, it was also necessary for the bulk $\alpha$-Cr + $\beta$-NiAl structure to become enriched in nickel. This enrichment is indicated by the movement of the diffusion path in a direction from the bulk $\alpha + \beta$ composition toward the 100% Ni corner of the ternary diagram. Such a movement represents nickel enrichment because it occurs at a constant Cr/Al atom ratio. The enrichment of nickel in the $\alpha + \beta$ structure ultimately led to a destabilization and subsequent transformation of the structure to $\gamma + \beta$. The $\gamma$-Ni and $\gamma$-Ni + $\beta$-NiAl layers continued to grow in a parabolic manner, indicating that their growth kinetics were both diffusion controlled. Indeed, the poor oxidation resistance of the $\alpha + \beta$ alloy could be attributed to the extensive internal $Al_2O_3$ formation, which in turn could be attributed to the oxidation-induced phase transformations which occurred.

Recent results[60] from a study on the oxidation behavior of TiAl + $(Ti,Nb)Al_3$ alloys at 1100°C in air provide an interesting example of the sensitivity of two-phase ternary alloys to selective oxidation processes. As summarized in Fig. 15, it was found that TiAl + $(Ti,Nb)Al_3$ alloys with a Ti/Nb atom ratio greater than ~1.9 formed a protective inner scale of $Al_2O_3$, while alloys with an atom ratio less than this value formed a nonprotective scale consisting of alternating $TiO_2 + Al_2O_3$–$AlNbO_4$ layers. The formation of a nonprotective scale could be attributed to the fact that, with the higher niobium content in the alloy, selective removal of Al and Ti due to oxidation caused the alloy phase equilibria to change from TiAl + $(Ti,Nb)Al_3$ to TiAl + $Nb_2Al$ which, in turn, resulted in the formation of the fast-growing oxide $AlNbO_4$ (the oxidation product which forms on

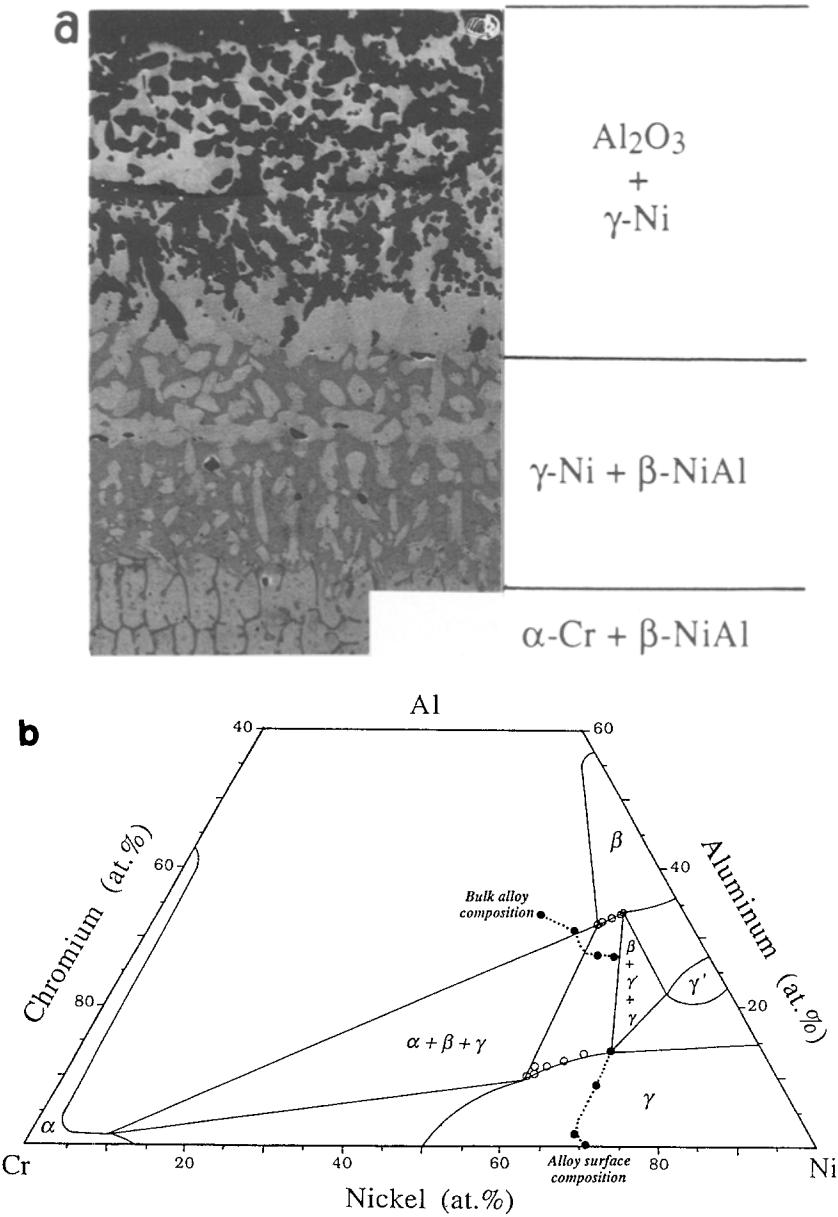


**Fig. 14.** (a) Backscattered electron image showing the microstructure of a $\beta$-NiAl + $\alpha$-Cr alloy after 136 one-hour oxidation cycles at 1100°C in still air. (b) The measured diffusion path of the alloy plotted in the Ni–Cr–Al phase diagram: closed symbols = local overall alloy composition; open symbols = individual phase composition.

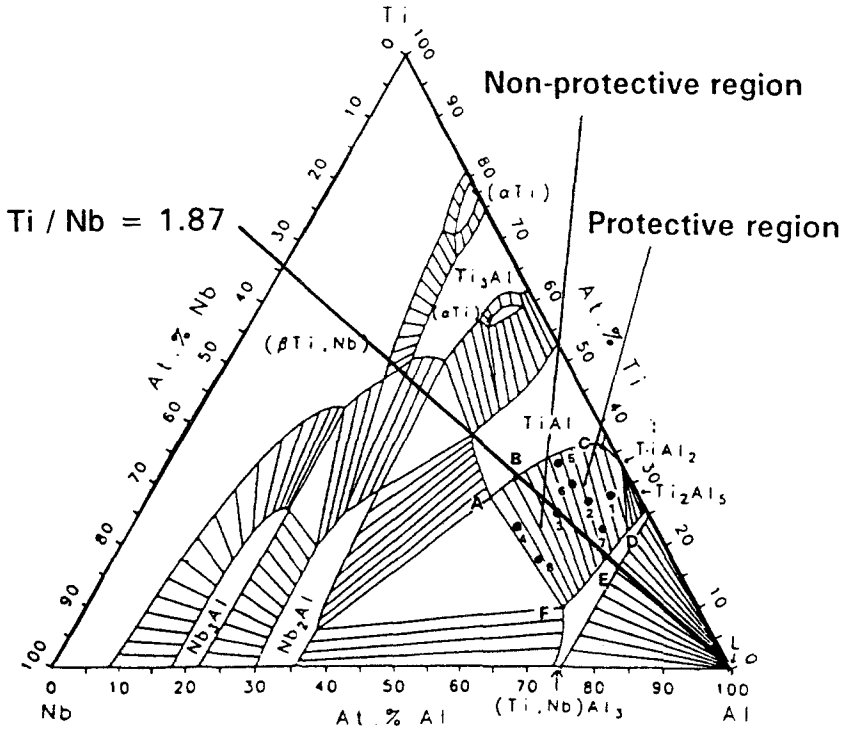


**Fig. 15.** Effect of alloy composition on the type of scaling behavior of TiAl + $(Ti,Nb)Al_3$ alloys.

the $Nb_2Al$ phase). Such a change in phase equilibria did not occur in alloys with a Ti/Nb atom ratio of greater than ~1.9 and, consequently, protective scale formation could occur.

On the basis of the qualitative nature of the preceding discussion, it is clear that more systematic experimental investigations are necessary in order to obtain a better understanding of the corrosion behavior of two-phase ternary alloys. Such investigations are warranted in view of the considerable practical importance of these types of alloys. Computational modeling is also required, although, the usefulness of a given model is inevitably dependent on the accuracy of the relevant input data. Therefore, a need also exists to conduct fundamental studies aimed at determining the various kinetic parameters associated with two-phase, ternary-alloy oxidation.

## SUMMARY

The present analysis has highlighted some of the important factors associated with the high-temperature corrosion of two-phase alloys. A most

important factor is the restriction that the presence of two metal phases imposes on the diffusion of the metal components in the alloy. Under certain conditions this may lead to peculiar scale structures, some of which are unknown or even impossible in single-phase alloys. Some general conclusions concerning the possible types of scale structures and the conditions for their appearance are presented for the binary systems, while the behavior of ternary systems is much more complex and for the moment can only be described by means of an analysis of the results of some practical investigations. In both cases there is a need of more systematic investigation of both practical and theoretical nature in order to improve the current understanding of these complex processes.

## ACKNOWLEDGMENTS

The authors gratefully acknowledge Campbell King for his help in the preparation of the figures.

## REFERENCES

1. P. Kofstad, *High Temperature Corrosion* (Elsevier Applied Science, London, 1988).
2. G. R. Wallwork, *Reps. Progr. Phys.* **39**, 401 (1976).
3. D. P. Whittle, in *High Temperature Corrosion*, R. A. Rapp, ed. (NACE, Houston, 1983), p. 171.
4. G. C. Wood and F. H. Stott, *Mater. Sci. Technol.* **3**, 519 (1987).
5. G. Wahl, *Thin Solid Films* **107**, 417 (1983).
6. J. Stringer, P. Corkish, and D. P. Whittle, in *Stress Effects on the Oxidation of Metals*, J. V. Cathcart, ed. (Met. Soc. AIME, New York, 1975), p. 75.
7. Ge Wang, B. Gleeson, and D. L. Douglass, *Oxid. Met.* **35**, 333 (1991).
8. Ge Wang, *J. Phys. IV*, Colloq. C9, suppl. *J. Phys. III* **3**, 873 (1993).
9. S. Ling, T. A. Ramanarayanan, and R. Petkovi-Luton, *Oxid. Met.* **40**, 179 (1993).
10. F. Gesmundo, F. Viani, Y. Niu, and D. L. Douglass, *Oxid. Met.* **39**, 197 (1993).
11. F. Gesmundo, F. Viani, Y. Niu, and D. L. Douglass, *Oxid. Met.* **40**, 373 (1993).
12. F. Gesmundo, F. Viani, Y. Niu, and D. L. Douglass, *Oxid. Met.* **42**, 465 (1994).
13. F. Gesmundo, F. Viani, and Y. Niu, *Oxid. Met.* **42**, 409 (1994).
14. F. Gesmundo, Y. Niu, and F. Viani, *Oxid. Met.* **43**, 379 (1995).
15. F. Gesmundo, Y. Niu, and F. Viani, *Oxid. Met.*, accepted for publication.
16. J. L. Smialek and G. H. Meier, in *Superalloys II*, C. T. Sims, N. S. Stoloff, and W. C. Hagel, eds. (Wiley, New York, 1987), p. 293.
17. G. T. Lai, *High-Temperature Corrosion of Engineering Alloys* (ASM, Materials Park, OH, 1990).
18. J. A. Nesbitt, N. S. Jacobson, and R. A. Miller, in *Surface Engineering*, Vol. II: *Technological Aspects*, R. Kossowsky, ed. (CRC Press, Boca Raton, FL, 1989), p. 25.
19. R. Dorolia, J. J. Lewandowski, C. T. Liu, P. L. Martin, D. B. Miracle, and M. V. Nathal, *Structural Intermetallics* (TMS, Warrendale, PA, 1993).
20. T. Grobstein and J. Doychak (eds.), *Oxidation of High-Temperature Intermetallics* (TMS, Warrendale, PA, 1988).
21. J. G. Smeggil, *Oxid. Met.* **9**, 31 (1975).
22. J. G. Smeggil, *Oxid. Met.* **9**, 225 (1975).
23. J. Stringer, D. M. Johnson, and D. P. Whittle, *Oxid. Met.* **12**, 257 (1978).
24. M. E. El Dahshan and M. I. Hazzaa, *Werkst. Korros.* **38**, 422 (1987).

25. F. H. Stott, G. C. Wood, and J. G. Fountain, *Oxid. Met.* **14**, 31 (1980).
26. L. V. Mallia and D. J. Young, *Oxid. Met.* **21**, 103 (1984).
27. N. Belen, P. Tomaszewicz, and D. J. Young, *Oxid. Met.* **22**, 227 (1984).
28. J. Doychak, J. A. Nesbitt, R. D. Noebe, and R. R. Bowman, *Oxid. Met.* **38**, 45 (1992).
29. D. E. Alman and N. S. Stoloff, in *High Temperature Silicides and Refractory Alloys*, Mat. Res. Soc. Symp. Proc. Vol. 322, C. L. Briant, J. J. Petrovic, B. P. Bewlay, A. K. Vasudvan, and H. A. Lipsitt, eds. (Materials Research Society, 1994), p. 255.
30. B. Gleeson, W. H. Cheung, and D. J. Young, *Corros. Sci.* **35**, 923 (1993).
31. S. Espevik, R. A. Rapp, P. L. Daniel, and J. P. Hirth, *Oxid. Met.* **20**, 37 (1983).
32. C. A. Barrett and C. E. Lowell, *Oxid. Met.* **11**, 199 (1977).
33. J. L. González Carrasco, P. Adeva, and M. Abell, *Oxid. Met.* **33**, 1 (1990).
34. J. A. Nesbitt and R. W. Heckel, *Oxid. Met.* **29**, 75 (1988).
35. G. P. Wagner and G. Simkovich, *Oxid. Met.* **27**, 157 (1987).
36. M. E. El Dahshan, J. Stringer, and D. P. Whittle, *Cobalt* **4**, 86 (1974).
37. V. Nagarajan, I. G. Wright, and J. Stringer, Proc. 12th Int. Plansee Seminar, 1989, p. 333.
38. I. G. Wright and V. Nagarajan, *J. Phys. IV*, Colloq. C9, suppl. *J. Phys. III* **3**, 151 (1993).
39. I. G. Wright, V. Nagarajan, and J. Stringer, *Corros. Sci.* **35**, 841 (1993).
40. X. L. Li, R. Hillel, F. Teyssandier, S. K. Choi, and F. J. J. Van Loo, *Acta Metall. Mater.* **40**, 3149 (1992).
41. G. Welsch and A. I. Kahveci, in *Oxidation of High-Temperature Intermetallics*, T. Grobstein and J. Doychak, eds. (TMS, Warrendale, PA, 1988), p. 207.
42. R. Petkovic-Luton and T. A. Ramanarayanan, *Oxid. Met.* **34**, 381 (1990).
43. C. Wagner, *J. Electrochem. Soc.* **99**, 369 (1952).
44. W. J. Quaddakers, N. Zheng, A. Gil and H. Nickel, in *Progress in the Understanding and Prevention of Corrosion*, J. M. Costa and A. D. Mercer, eds. (Inst. of Materials, London, 1993), Vol. 1, p. 770.
45. R. Durham, B. Gleeson, and D. J. Young, unpublished research, The University of New South Wales, Australia.
46. M. Castro Rebelo, Y. Niu, F. Rizzo, and F. Gesmundo, *Oxid. Met.* **43**, 561 (1995).
47. M. J. Monteiro, Y. Niu, F. Rizzo, and F. Gesmundo, *Oxid. Met.* **43**, 527 (1995).
48. F. Gesmundo, P. Nanni, and D. P. Whittle, *J. Electrochem. Soc.* **127**, 1773 (1980).
49. R. A. Rapp, *Corrosion* **21**, 382 (1965).
50. F. Gesmundo, P. Nanni and F. Viani, *Proc. 9th Internat. Symp. on Reactivity of Solids* (Elsevier, Amsterdam, 1982), Vol. 1, p. 151.
51. Y. Niu, F. Gesmundo, F. Viani, and D. L. Douglass, *Oxid. Met.* accepted for publication.
52. B. Gleeson, D. L. Douglass, and F. Gesmundo, *Oxid. Met.* **31**, 209 (1989).
53. G. Wang, R. Carter, and D. L. Douglass, *Oxid. Met.* **32**, 273 (1989).
54. Y. Niu, F. Gesmundo, and F. Viani, *Corros. Sci.* **36**, 423 (1994).
55. Y. Niu, F. Gesmundo, and F. Viani, *Corros. Sci.* **36**, 853 (1994).
56. R. T. DeHoff, *Thermodynamics in Materials Science* (McGraw-Hill, New York, 1993), p. 214.
57. B. Gleeson, D. L. Douglass, and F. Gesmundo, *Oxid. Met.* **34**, 123 (1990).
58. M. P. Brady, R. J. Hanrahan, and E. D. Verink, in *Processing and Fabrication of Advanced Materials for High Temperature Applications—II*, V. A. Ravi and T. S. Srivatsan, eds. (TMS, Warrendale, PA, 1993), p. 419.
59. M. P. Brady, R. J. Hanrahan, S. P. Randall, and E. D. Verink, *Scripta Metall.* **28**, 115 (1993).
60. D. Yang and B. Gleeson, unpublished research, The University of New South Wales, Australia.